

# Quantitative evaluation of contrast agent uptake in standard fat-suppressed dynamic contrast-enhanced MRI examinations of the breast

Evanthia Kousi<sup>a),\*</sup>

CR-UK and EPSRC Cancer Imaging Centre, Royal Marsden NHS Foundation Trust, Institute of Cancer Research, Sutton, Surrey SM2 5PT, UK

Joely Smith\*

Brighton and Sussex University Hospitals NHS Trust, Brighton BN2 5BE, UK

Araminta E. Ledger and Erica Scurr

CR-UK and EPSRC Cancer Imaging Centre, Royal Marsden NHS Foundation Trust, Institute of Cancer Research, Sutton, Surrey SM2 5PT, UK

Steven Allen and Robin M. Wilson

Department of Radiology, Royal Marsden NHS Foundation Trust, Chelsea, London SW3 6JJ, UK

Elizabeth O'Flynn

CR-UK and EPSRC Cancer Imaging Centre, Royal Marsden NHS Foundation Trust, Institute of Cancer Research, Sutton, Surrey SM2 5PT, UK

Romney J.E. Pope

Department of Radiology, Royal Marsden NHS Foundation Trust, Chelsea, London SW3 6JJ, UK

Martin O. Leach and Maria A. Schmidt

CR-UK and EPSRC Cancer Imaging Centre, Royal Marsden NHS Foundation Trust, Institute of Cancer Research, Sutton, Surrey SM2 5PT, UK

(Received 4 November 2016; revised 24 October 2017; accepted for publication 24 October 2017; published 30 November 2017)

**Purpose:** To propose a method to quantify  $T_1$  and contrast agent uptake in breast dynamic contrast-enhanced (DCE) examinations undertaken with standard clinical fat-suppressed MRI sequences and to demonstrate the proposed approach by comparing the enhancement characteristics of lobular and ductal carcinomas.

**Methods:** A standard fat-suppressed DCE of the breast was performed at 1.5 T (Siemens Aera), followed by the acquisition of a proton density (PD)-weighted sequence, also fat suppressed. Both sequences were characterized with test objects ( $T_1$  ranging from 30 ms to 2,400 ms) and calibration curves were obtained to enable  $T_1$  calculation. The reproducibility and accuracy of the calibration curves were also investigated. Healthy volunteers and patients were scanned with Ethics Committee approval. The effect of  $B_0$  field inhomogeneity was assessed in test objects and healthy volunteers. The  $T_1$  of breast tumors was calculated at different time points (pre-, peak-, and post-contrast agent administration) for 20 patients, pre-treatment (10 lobular and 10 ductal carcinomas) and the two cancer types were compared (Wilcoxon rank-sum test).

**Results:** The calibration curves proved to be highly reproducible (coefficient of variation under 10%).  $T_1$  measurements were affected by  $B_0$  field inhomogeneity, but frequency shifts below 50 Hz introduced only 3% change to fat-suppressed  $T_1$  measurements of breast parenchyma in volunteers. The values of  $T_1$  measured pre-, peak-, and post-contrast agent administration demonstrated that the dynamic range of the DCE sequence was correct, that is, image intensity is approximately directly proportional to  $1/T_1$  for that range. Significant differences were identified in the width of the distributions of the post-contrast  $T_1$  values between lobular and ductal carcinomas ( $P < 0.05$ ); lobular carcinomas demonstrated a wider range of post-contrast  $T_1$  values, potentially related to their infiltrative growth pattern.

**Conclusions:** This work has demonstrated the feasibility of fat-suppressed  $T_1$  measurements as a tool for clinical studies. The proposed quantitative approach is practical, enabled the detection of differences between lobular and invasive ductal carcinomas, and further enables the optimization of DCE protocols by tailoring the dynamic range of the sequence to the values of  $T_1$  measured. © 2017 The Authors. *Medical Physics* published by Wiley Periodicals, Inc. on behalf of American Association of Physicists in Medicine. [https://doi.org/10.1002/mp.12652]

Key words: breast, breast cancer, calibration, DCE-MRI, quantification

## 1. INTRODUCTION

Dynamic Contrast-Enhanced MRI (DCE-MRI) is a powerful clinical tool for the detection, diagnosis, and staging of the breast cancer.<sup>1,2</sup> Following the administration of a gadolinium chelate contrast agent, tissue perfusion can be estimated using changes in the signal intensity over time on a series of images obtained with fast 3D  $T_1$ -weighted pulse sequences. Clinical DCE-MRI examinations of the breast are commonly performed with fat suppression and provide time-signal intensity curves to qualitatively assess the enhancement kinetics of the contrast agent uptake in tumors. In contrast, pharmacokinetic modeling offers a quantitative approach to investigate tumor vascularity associated with malignancy and has been shown to improve the diagnostic performance of MRI as well as the prediction of treatment response.<sup>3–5</sup> In this setting, a separate proton density sequence is used as a reference, enabling the calculation of  $T_1$ . Pharmacokinetic modeling requires rapid data acquisitions, sacrificing spatial resolution and breast coverage, and is not currently a part of the standard clinical practice.

The breast MRI is recommended for the assessment of biopsy-proven invasive lobular carcinomas (ILCs). This is due to the lower diagnostic performance of other imaging modalities in accurately defining the extent of disease,<sup>6,7</sup> which can be caused by the diffuse growth pattern of some ILCs. Differences in the DCE-MRI enhancement characteristics between ILCs and invasive ductal carcinomas (IDCs) have been previously demonstrated.<sup>8,9</sup>

In this work, we propose to combine a high-resolution fat-suppressed clinical DCE-MRI sequence with the ability to perform quantitative  $T_1$  measurements by introducing a proton density-weighted sequence as a reference. We demonstrate our method by comparing the enhancement characteristics of two groups of breast patients: ILCs and IDCs. In addition, we evaluate the accuracy and reproducibility of the obtained  $T_1$  values. Furthermore, we show that the dynamic range of our DCE-MRI sequence is suited to the range of  $T_1$  values measured in our clinical breast examinations, enabling contrast agent uptake to be correctly depicted.

## 2. METHODS

### 2.A. Imaging protocol

Subjects were scanned at 1.5 T (Aera, Siemens, Erlangen, Germany) using an eight-channel breast receiver coil. Volunteers were scanned with an approval of the Research Ethics Committee (UK NHS HRA/NRES Committee London-Chelsea 1406/18-06-1997) and written consent was obtained. The retrospective analysis of patient studies was approved by the Research Ethics Committee (“Evaluation of Breast MRI Protocols”, Service Evaluation). A standard clinical breast DCE-MRI protocol was performed using spectrally selective (Spectral Attenuated Inversion Recovery, SPAIR) pulses for fat suppression and three-dimensional (3D)  $T_1$ -weighted spoiled gradient-echo sequences (TE/TR = 2/4.5 ms, flip angle = 18°, pixel size = 1.31 × 1.31 × 1 mm, parallel

imaging factor 2, number of slices = 160, acquisition matrix = 290 × 320, FOV = 380 × 420 mm<sup>2</sup>). The readout gradient direction was anterior/posterior to minimize cardiac motion artifacts over the breasts. A single dose of contrast agent (Dotarem, Guerbet, France) was administered at 2–3 mL/s (MedRad, USA) depending on the size of the largest vascular access device that could be fitted to the patient. One pre- and eight post-contrast transaxial 3D data sets were acquired in 56 s each, in agreement with the current national guidelines.<sup>10</sup> A proton density (PD)-weighted sequence was subsequently obtained with identical parameters to the DCE-MRI sequence using a lower flip angle of 4°.

### 2.B. Quantitative assessment of contrast agent uptake

In quantitative DCE examinations undertaken for pharmacokinetic modeling,  $T_1$  is calculated from a combination of the two data sets obtained with differing amounts of  $T_1$  weighting (spoiled gradient echoes with high and low flip angles).<sup>11</sup> The sequence with the high flip angle is  $T_1$  weighted while the sequence with low flip angle has minimal  $T_1$  weighting. The concentration of contrast agent in each voxel is calculated quantitatively from  $T_1$  values:

$$[\text{Gd}] = (1/T_1 - 1/T_{1\text{pre}})/r \quad (1)$$

where  $T_{1\text{pre}}$  is the native  $T_1$  of the tissue and  $r$  is the relaxivity of the administered contrast agent.

Although an analytical solution of the Bloch equations is not usually practical for the fat-suppressed spoiled gradient-echo sequences used in DCE, these sequences follow the same principles and both experimental work and numerical simulations demonstrate fat-suppressed and non-fat-suppressed sequences have similar contrast characteristics: image intensity should be proportional to  $1/T_1$  over the  $T_1$  range of interest.<sup>12</sup> Therefore, subtracting a post-contrast image ( $S_1$ ) from the pre-contrast baseline ( $S_{\text{pre}}$ ) demonstrates the contrast agent uptake qualitatively. However, even in a perfect system with no changes in image intensity associated with imperfect excitation or receiver coil sensitivity, quantitative analysis is not possible because there will be (a) variations of image intensity in the same examination associated with differences in the proton density (equilibrium magnetization) from voxel to voxel and (b) changes to coil filling factor and changes to system gain which makes it impossible to compare directly an examination to another or a patient to another.

It is possible to define an enhancement ratio (ER) as:

$$\text{ER} = (S_1 - S_{\text{pre}})/S_{\text{pre}} \quad (2)$$

As a ratio, ER is not affected by proton density or by coil sensitivity, but is affected by the native  $T_1$  value. Variations in ER within a lesion may not relate to different contrast agent uptake, but simply to different native  $T_1$  values; the same applies to longitudinal changes in a patient study. ER is only semiquantitative. This is the main motivation to develop a method to calculate  $T_1$  using fat-suppressed sequences.

To calculate  $T_1$ , we introduce a low flip angle image which is practically proton density weighted and also fat suppressed. Using two sequences with different  $T_1$  weighting, we calculate  $T_1$  post-contrast for each pixel. For that purpose, the behavior of each sequence is studied with a test object comprising a very wide range of  $T_1$  values, and empirical curves are used, instead of the solution of the Bloch equations.<sup>11</sup>

In a similar way to pharmacokinetic studies, we related the DCE/PD image ratio to the  $T_1$  value using an experimental measurement on test objects to provide a calibration curve. This method provided a direct measurement of the  $T_1$  value at the end of the DCE protocol; the last frame of the DCE and the PD acquisition are used jointly to calculate  $T_1$  ( $T_{1\text{post}}$ ). This approach presumes a slow clearance of the contrast agent from the patient's system between the last DCE and PD acquisitions, and therefore, no significant changes in the contrast agent concentration are expected over those few minutes. In order to calculate  $T_1$  values in previous frames, we used the same principles employed in quantitative DCE examinations (without fat suppression); we presumed that all changes of image intensity were associated with  $T_1$  (i.e., there was no change to the equilibrium magnetization; there were no other hardware changes; and the signal intensity for DCE was a known function of  $T_1$ ).

### 2.C. Test objects

Plastic tubes filled with aqueous solutions of  $\text{CuSO}_4$  of different concentrations were used to generate the calibration curves. Standard Inversion Recovery (IR) measurements were employed to provide the reference values for this test object, comprising  $T_1$  values within the range 30 ms–2,600 ms. These solutions were scanned with the DCE and PD sequences to produce a curve representing the ratio between the image intensity obtained with DCE and PD images, now referred to as image ratio, as a function of  $R_1 = 1/T_1$ . A separate curve was calculated to provide calibrated image intensity values for the imaging sequences also as a function of  $R_1$ . A least-square smooth spline line fitting was performed using R statistical software (R v.3.0.2, www.r-project.org) and the % coefficient of variation was used to evaluate the reproducibility of the calibration curves. The DCE pulse sequence employed has a short TE, and therefore, we do not expect the contrast to have  $T_2$ —or  $T_2^*$ —weighting for the test objects used in calibration and for the breast.

This measurement was repeated on two different occasions separated by 4 months to calibrate the  $T_1$  measurement and to evaluate the stability of the calibration curves. For this measurement, the power applied by the fat suppression SPAIR pulse was set to zero, and therefore, the calibration curves were not affected by  $B_0$  inhomogeneity.

The effect of  $B_0$  inhomogeneity was investigated separately, with the same set of solutions. The central frequency was changed in four steps of 50 Hz in both directions ( $-200 \text{ Hz} < \omega_0 < 200 \text{ Hz}$ ), and therefore, the applied fat suppression pulse partially suppressed water signals. Errors in  $T_1$  measurements were attributed to off-resonance effects.

In addition, a uniform test object ( $T_1 \sim 110 \text{ ms}$ ) was scanned with the same sequences to verify whether the ratio between DCE and PD images was constant over the breast volume, as this could be affected by  $B_1$  inhomogeneity<sup>13</sup> and uniformity filters.<sup>14</sup> The percent ratio image uniformity (PRIU) was calculated over the coil volume to be occupied by the breasts according to the following equation:

$$PRIU = 100 \times \left( 1 - \frac{Ratio_{max} - Ratio_{min}}{Ratio_{max} + Ratio_{min}} \right) \quad (3)$$

### 2.D. Clinical examinations

The DCE examinations of 20 patients with histologically confirmed breast tumors were analyzed. Tumors comprised ten lobular carcinomas [six grade 2 ILCs, four lobular carcinomas in situ (LCIS)] and ten ductal carcinomas [two grade 1, five grade 2, and one grade 3 IDCs, two high-grade ductal carcinomas in situ (DCIS)]. All post-contrast 3D data sets were registered to the pre-contrast data set prior to analysis using a rigid registration method with six degrees of freedom (3D Slicer v. 4.4.0, www.slicer.org). The largest transaxial cross section for each tumor was chosen and the tumor outline performed using in-house software (IDL 8.4 Boulder, CO, USA) and was approved by a specialist breast Radiologist.

In addition, DCE and PD data sets were obtained for two healthy volunteers by changing the central frequency in steps of 25 Hz in order to investigate further the off-resonance effects on clinical  $T_1$  calculations. The fibroglandular tissue was segmented using the k-means clustering algorithm over the entire breast volume (IDL 8.4 Boulder, CO, USA).

The  $T_1$  relaxation time of the tumors was calculated on a pixel-by-pixel basis using the test object calibration curves at three time points: (a) before contrast administration ( $T_{1\text{pre}}$ ), (b) at peak-contrast uptake, that is, the shortest  $T_1$  ( $T_{1\text{peak}}$ ), and (c) the post-contrast (final) frame of the DCE examination ( $T_{1\text{post}}$ ). In cases of late tumor enhancement,  $T_{1\text{peak}} = T_{1\text{post}}$ . Gadolinium concentration [Gd] and the %ER of the tumors were also calculated pixel-by-pixel at peak- and post-enhancement frames, using Eqs. (1) and (2), respectively. The following characteristics of lobular and ductal carcinomas were compared: peak-enhancement frame, median, and interquartile range (IQR) of the  $T_1$  values at the pre-, peak-, and the post-enhancement frames, and of [Gd] and %ER at peak- and post-enhancement. The Wilcoxon rank-sum test was used for statistical analysis with a significance level of  $P < 0.05$  (R v.3.0.2, www.r-project.org).

## 3. RESULTS

### 3.A. Test object study

Figure 1 shows the calibration curves produced using phantom data for the clinical pulse sequences on two separate occasions. Calibration curves were produced for the ratio image intensity [Fig. 1(a)] and the DCE image intensity [Fig. 1(b)]. The image intensity of the DCE sequence can be

considered approximately directly proportional to  $R_1$  for  $R_1 < 0.01 \text{ ms}^{-1}$  (or  $T_1 > 100 \text{ ms}$ ). The calibration curves proved to be reproducible: the calculated coefficient of variation for different  $T_1$  values varied from 0.1% to 9% for the ratio image and 0.5%–10% for the DCE image. Fat-suppressed  $T_1$  measurements were in agreement with IR measurements for the test objects [Fig. 1(c)]: the average absolute difference between fat-suppressed  $T_1$  measurements and IR measurements of the test tube solutions was 7% (range 0.28%–16%); the largest difference was found for the longest  $T_1$  (2600 ms).

The curves in Figs. 1(a) and 1(b) are affected by off-resonance effects if field inhomogeneity causes the fat suppression pulse to suppress water. Frequency shifts under 50 Hz introduced changes up to 19% to  $T_1$  measurements in the range  $100 \text{ ms} < T_1 < 1000 \text{ ms}$ . Figure 2 shows DCE and ratio images of tube solutions, with  $T_1$  ranging from 30 ms to 2400 ms, as a function of frequency shift demonstrating a progressive suppression of water signal that results in distorted calibration curves. In volunteer studies,  $T_1$  values obtained for normal breast parenchyma showed small variations (< 3%) for frequency shifts below 50 Hz. The  $T_1$  of the breast parenchyma was also measured on a set of patients with unilateral disease (Appendix 1).

Figure 3 shows a transaxial slice of a uniform test object acquired with DCE [Fig. 3(a)] and PD [Fig. 3(b)] sequences and the ratio between them [Fig. 3(c)]. Ratio image is uniform over the coil volume that is occupied by small or large breasts ( $\text{PRIU}_{\text{Right Coil}} = 93\%$  and  $87\%$ , respectively,  $\text{PRIU}_{\text{Left Coil}} = 91\%$  and  $90\%$ , respectively), suggesting only relatively small errors associated with spatial variations in  $B_0$  and  $B_1$ .

### 3.B. Clinical study

Figure 4 shows the pre-, peak-, and the post-contrast enhancement frames of two breast examinations, followed by

the image with low flip angle (PD) and the corresponding  $R_1$  measurements using the test object calibration curves. The % ER was also calculated pixel-by-pixel using Eq. (2) and compared with [Gd] post-enhancement [Eq. (1)]. The graphs show that although both cases have the same ER range, the range of values for the gadolinium concentration is different. Axes have been scaled equally to highlight this observation.

Median  $T_1$ , [Gd], and %ER values were calculated for every patient; mean  $\pm$  standard deviation is shown in Table I. There were no significant differences between the two cancer groups ( $P > 0.05$ ,  $P$  values in Table I). Peak-enhancement occurred in the final frame for four (three ILC and one LCIS) of ten lobular carcinomas suggesting slower uptake of the contrast agent for these tumors. Although peak-enhancement occurred earlier for nine of ten ductal carcinomas, this difference was not significant ( $P = 0.8$ , Table I). There were no statistically significant differences in IQR for  $T_{1\text{pre}}$ ,  $[\text{Gd}]_{\text{peak}}$ ,  $[\text{Gd}]_{\text{post}}$ ,  $\%ER_{\text{peak}}$ , and  $\%ER_{\text{post}}$  between the two cancer groups ( $P > 0.05$ ,  $P$  values in Table II), but the  $T_1$  IQR was significantly higher for lobular carcinomas in peak- and post-enhancement frames ( $P < 0.05$ ,  $P$  values in Table II).

Global  $T_1$  histograms (100 ms bin size) for the pre-, peak-, and post-contrast enhancement frames are shown in Fig. 5. The number of voxels in the first bin ( $T_1 \leq 100 \text{ ms}$ ) falling to the nonlinear part of the calibration curves (Fig. 1) was 0, 18, and 16 for  $T_{1\text{pre}}$ ,  $T_{1\text{peak}}$ , and  $T_{1\text{post}}$ , that is, no more than 0.4% of the total number of tumor voxels (4029). Therefore, the obtained  $T_1$  values demonstrate that the dynamic range of our DCE sequence suits the range of the  $T_1$  values measured in clinical examinations before and after contrast administration; the range of the  $T_1$  values for our cohort falls within the range, for which the image intensity is approximately directly proportional to  $1/T_1$  (or  $R_1$ ) for our DCE sequence (Fig. 1). The distribution of the native  $T_1$  values ( $T_{1\text{pre}}$ ) is similar

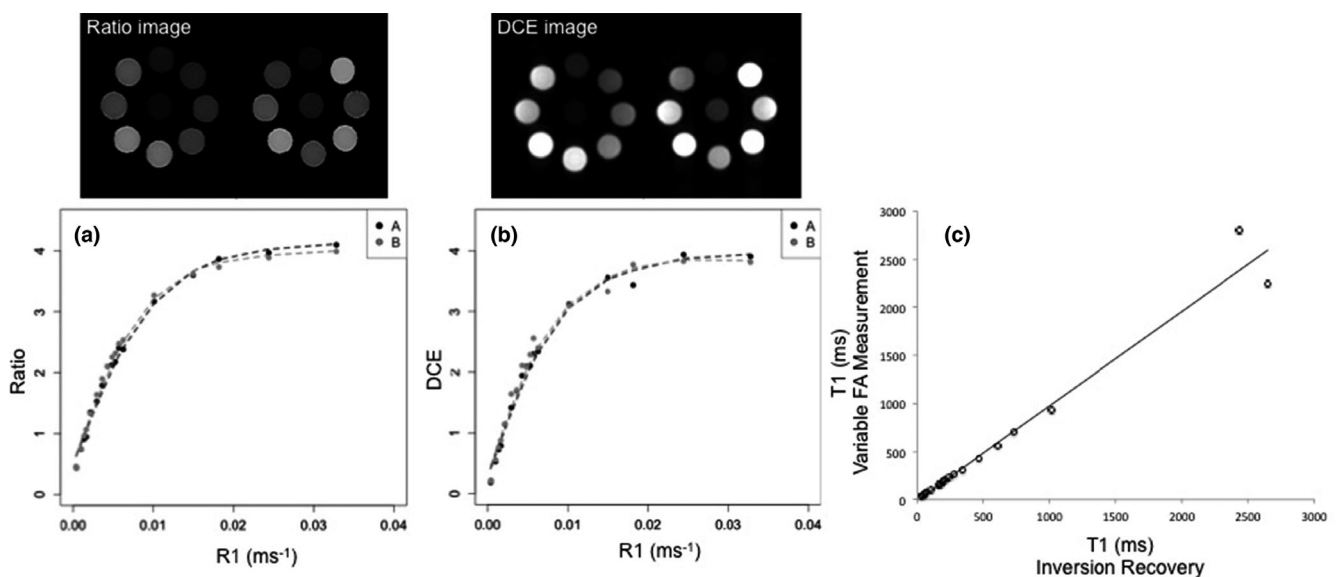


FIG. 1. Calibration curves as measured in two separate occasions, A (black) and B (grey): ratio (a) and DCE (b) image intensity as a function of  $R_1$  ( $\text{ms}^{-1}$ ) for test objects with  $T_1$  ranging from 30 ms to 2600 ms. (c) Fat-suppressed  $T_1$  measurements agree with the IR measurements for the test objects.



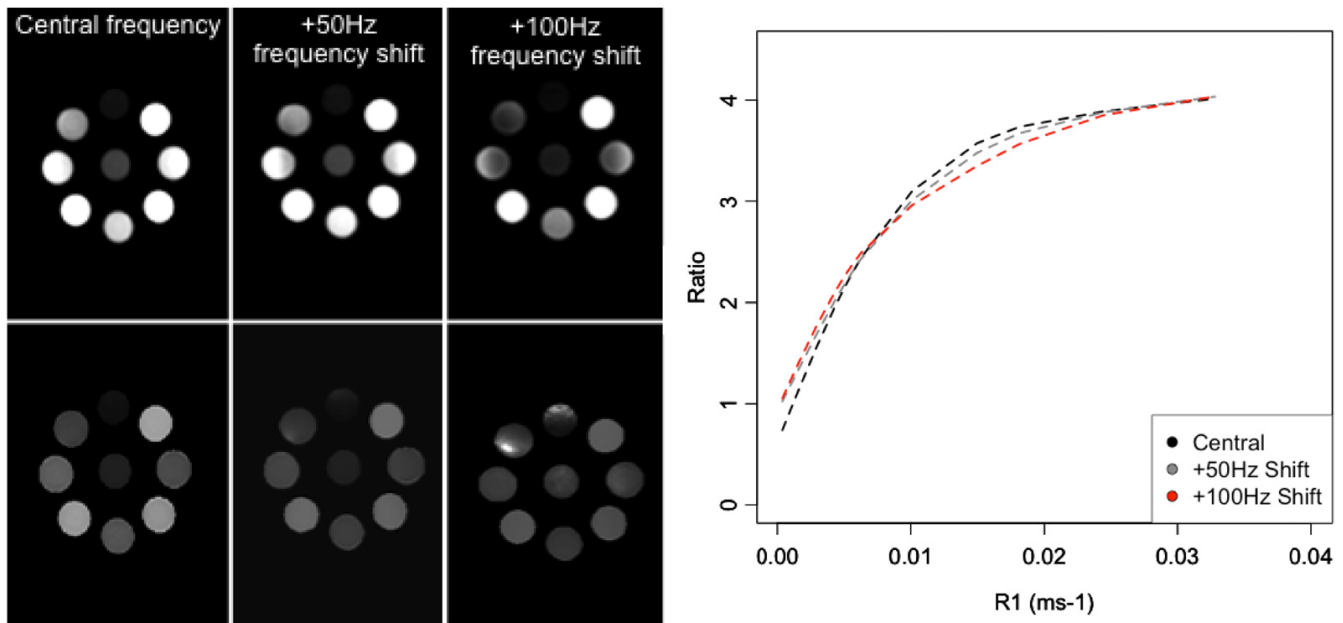


FIG. 2. Test objects ( $T_1$  range 30–2400 ms) DCE (top row) and ratio (bottom row) images acquired with different resonance frequencies showing errors being introduced by a gradual suppression of the water signal resulting in distorted calibration curves (right). [Color figure can be viewed at [wileyonlinelibrary.com](http://wileyonlinelibrary.com)]

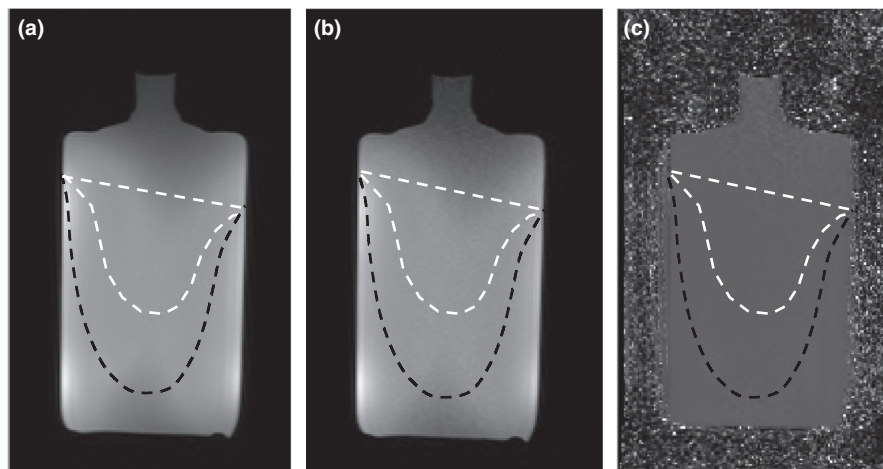


FIG. 3. Transaxial slice at the center of a uniform test object acquired with DCE (a) and PD sequences (b) and the corresponding ratio image (c). The right side of the breast coil is shown. High intensity uniformity of the ratio image is demonstrated over the coil area that is occupied by the breast. Dashed lines show the area at the center of the breast coil that is occupied by a small (white dashed line) or large (black dashed line) breast.

between lobular and ductal carcinomas [Fig. 5(a)], whereas the distributions of the  $T_1$  values after the contrast administration ( $T_{1\text{peak}}$  and  $T_{1\text{post}}$ ) suggest greater enhancement variability for the lobular carcinomas [Figs. 5(b) and 5(c)].

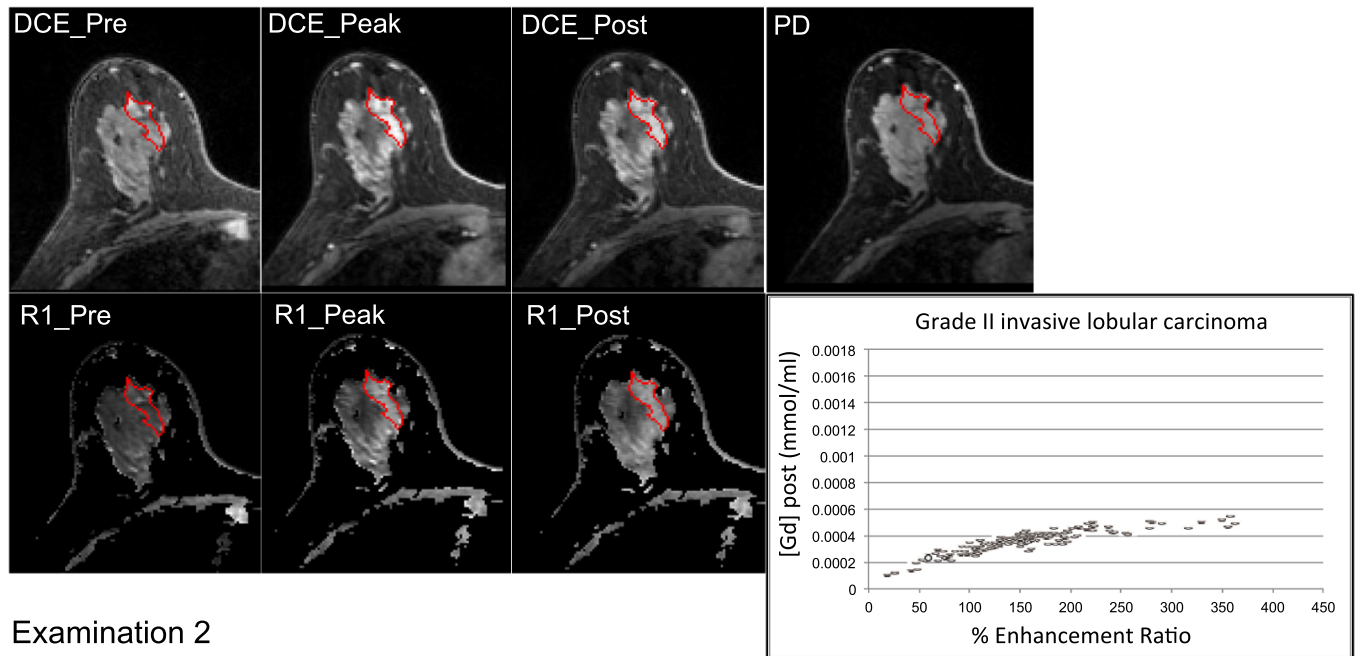
#### 4. DISCUSSION

The value of quantitative measurements in breast has already been demonstrated in the context of pharmacokinetic modeling. Using a small number of patients, we demonstrated a method to assess  $T_1$  in clinical fat-suppressed DCE-MRI examinations, thus quantifying contrast agent uptake. The proposed quantitative approach broadens the scope of the clinical DCE examination, is practical and achievable on any clinical MRI system, as it simply requires a calibration

with test objects. At this stage, the  $T_1$  calculations are performed off-line, but they could be easily integrated as a post-processing step. The use of quantitative methods enables direct comparisons of examinations in a longitudinal patient study or examinations from different patients; quantitative parameters such as  $T_1$  (pre- and post-contrast) and contrast agent concentration can be measured separately. The semi-quantitative enhancement ratio, in contrast, is affected by both  $T_1$  and contrast-agent concentration and is therefore more difficult to interpret signal changes relate to the baseline image intensity in a  $T_1$ -weighted acquisition.

In addition to proposing and demonstrating a novel approach to quantitative breast MRI, we also demonstrated that the dynamic range of our DCE pulse sequence is suitable for our clinical workload; the image intensity is

## Examination 1



## Examination 2

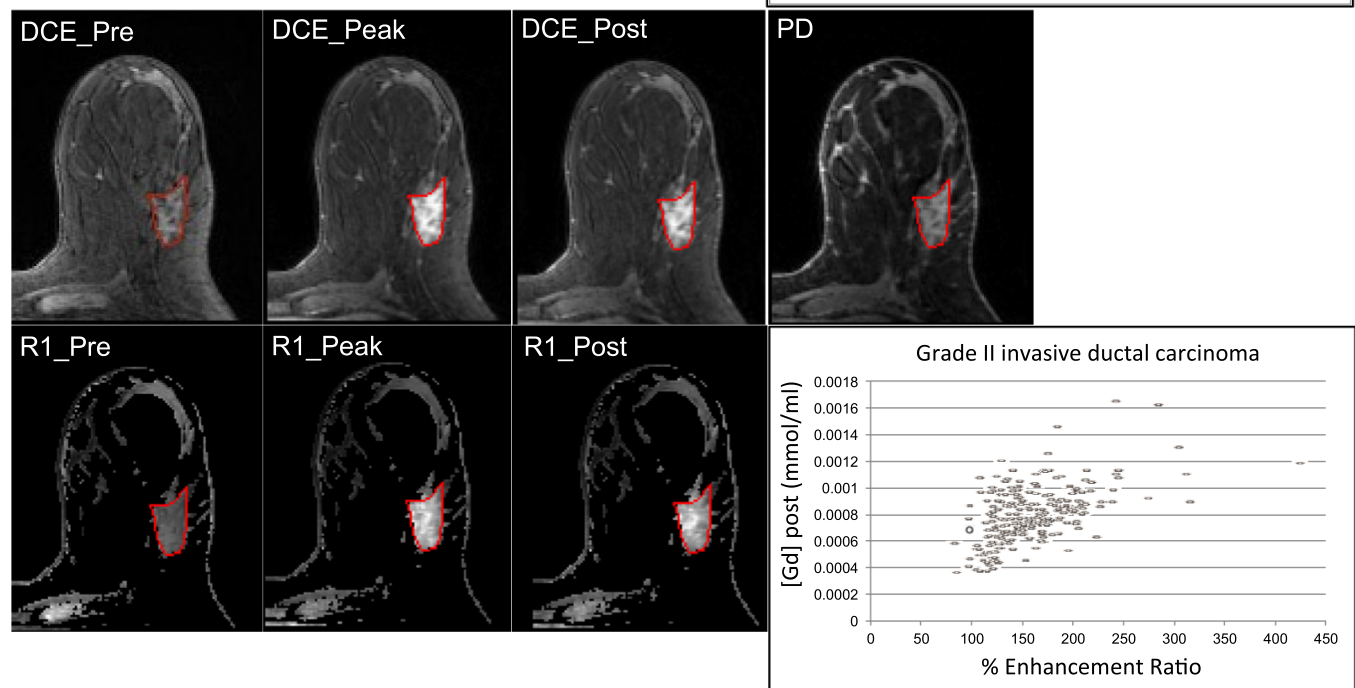


FIG. 4. Pre-, peak-, and post-contrast enhancement images followed by the corresponding PD images and R<sub>1</sub> maps of a grade II invasive lobular carcinoma (Examination 1) and grade II invasive ductal carcinoma (Examination 2); the mean native T<sub>1</sub> ± standard deviation for examinations 1 and 2 is 1311 ± 298 ms and 750 ms ± 139 ms, respectively. Graphs relate the % Enhancement ratio and [Gd] for these examinations. Only in the first example, the [Gd] rises monotonically with the Enhancement Ratio, in the second example, a more complex relationship is mediated by variations in native T<sub>1</sub>. R<sub>1</sub> maps for examinations 1 and 2 have been scaled independently. Within individual examinations, R<sub>1</sub> maps have been scaled equally. [Color figure can be viewed at [wileyonlinelibrary.com](http://wileyonlinelibrary.com)]

approximately directly proportional to  $1/T_1$  over the range of T<sub>1</sub> values we measured in breast lesions. Considering that the national guidelines for the breast screening program require that the contrast characteristics of the DCE sequence are evaluated,<sup>10</sup> it is essential to provide methods to do so. To the best of our knowledge, this article is the first to demonstrate that the DCE contrast characteristics are correct for the actual range of T<sub>1</sub> values found in clinical practice within our

patient population, taking into account specific constraints such as the rate of injection, the contrast agent dose and type, for example, which may vary in different populations.

Inaccurate T<sub>1</sub> measurements can be caused by the spatial variation in flip angle as a result of B<sub>1</sub> field inhomogeneity<sup>13</sup> and inaccurate RF transmitter power calibration. The use of uniformity filters in clinical examinations is also a factor that could potentially introduce errors,

TABLE I. Mean  $\pm$  standard deviation of median  $T_1$ , [Gd], and %ER across the different time points and median peak-enhancement frame for the lobular and ductal cancer groups.

Tumor group	$T_{1pre}$ (ms)	$T_{1peak}$ (ms)	$T_{1post}$ (ms)	$[Gd]_{peak}$ ( $\times 10^{-4}$ mmol/ml)	$[Gd]_{post}$ ( $\times 10^{-4}$ mmol/ml)	%ER <sub>peak</sub>	%ER <sub>post</sub>	Peak-enhancement frame
Lobular carcinomas (n = 10)	1275 $\pm$ 623	587 $\pm$ 367	591 $\pm$ 363	3.9 $\pm$ 2.2	3.9 $\pm$ 2.3	116 $\pm$ 33	114 $\pm$ 33	5 (4–8)
Ductal carcinomas (n = 10)	1087 $\pm$ 471	477 $\pm$ 193	494 $\pm$ 201	3.9 $\pm$ 1.9	3.7 $\pm$ 1.7	118 $\pm$ 32	111 $\pm$ 27	6 (3–8)
P-value	0.9	1	1	0.8	1	1	1	0.8

TABLE II. Mean  $\pm$  standard deviation of IQR  $T_1$ , [Gd], and %ER for the lobular and ductal cancer groups across the different time points.

Tumor group	IQR $T_{1pre}$ (ms)	IQR $T_{1peak}$ (ms)	IQR $T_{1post}$ (ms)	IQR $[Gd]_{peak}$ ( $\times 10^{-4}$ mmol/ml)	IQR $[Gd]_{post}$ ( $\times 10^{-4}$ mmol/ml)	IQR % ER <sub>peak</sub>	IQR % ER <sub>post</sub>
Lobular carcinomas (n = 10)	388 $\pm$ 251	206 $\pm$ 110	200 $\pm$ 118	2.1 $\pm$ 1.3	2.4 $\pm$ 2.4	62 $\pm$ 29	57 $\pm$ 25
Ductal carcinomas (n = 10)	251 $\pm$ 110	108 $\pm$ 39	113 $\pm$ 48	1.5 $\pm$ 0.7	1.5 $\pm$ 0.7	49 $\pm$ 12	48 $\pm$ 10
P-value	0.14	<b>0.02</b>	<b>0.04</b>	0.58	0.77	0.43	0.68

Bold values indicate significant differences.

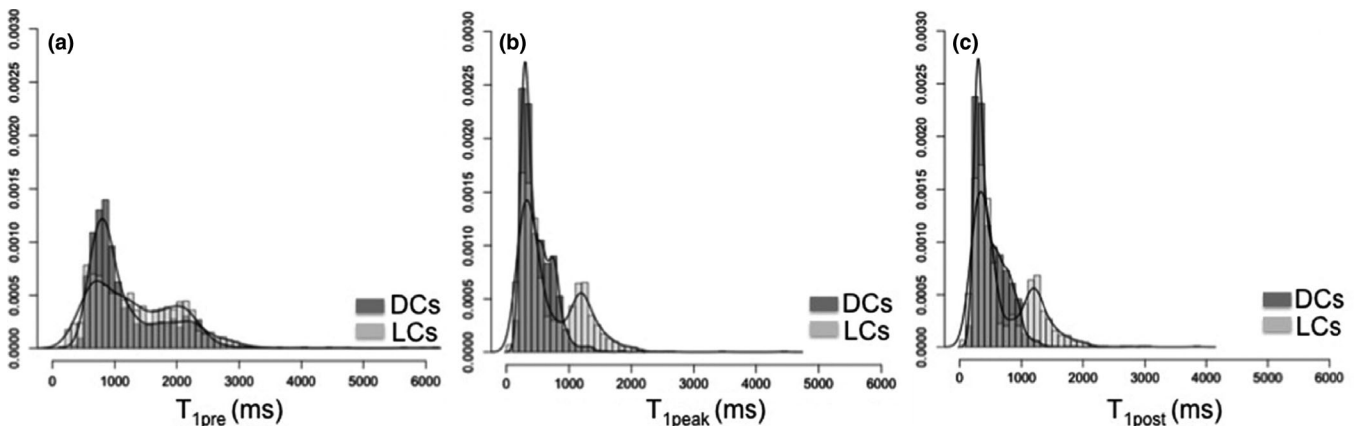


FIG. 5. Lobular carcinoma (LC) and ductal carcinoma (DC)  $T_1$  distributions with the corresponding distribution lines for the pre-, peak-, and post-contrast phases. The bimodal distribution of the post-enhancement  $T_1$  values observed for LC simply shows the uptake variation in the analyzed cases.

decreasing the level of confidence in quantification studies. These filters have shown to alter noise distribution resulting in SNR changes.<sup>14</sup> Although  $B_1$  inhomogeneity is more pronounced at higher fields ( $\geq 3$  T), all the aforementioned sources of error affect both standard  $T_1$  calculations in pharmacokinetic modeling and fat-suppressed  $T_1$  measurements.  $B_0$  variations are an additional issue, specific to breast DCE with fat suppression; good  $B_0$  homogeneity is required to avoid suppression of water signals. In this study, these main factors to affect accuracy of the  $T_1$  values obtained with the proposed method were investigated thoroughly. Calibration curves proved to be highly reproducible and a good agreement between IR and fat-suppressed  $T_1$  measurements was demonstrated; the discrepancy found for very long  $T_1$  values is probably due to a lower SNR. Spatial variation of the  $B_1$  field was investigated with a uniform test object.  $B_1$  inhomogeneity and the use of uniformity filters were found not to affect

significantly the  $T_1$  calculation over the breast volume for our 1.5 T system in a conductive test object.  $B_0$  inhomogeneity was simulated altering the central frequency. Small frequency variations introduce calibration errors if the water signal is suppressed, but unintentional water suppression is relatively rare.<sup>15</sup> Recent developments in shimming are encouraging<sup>16</sup> and will in general lead to improved performance in commercial systems. A separate issue is that DCE images may have fat and water out of phase; in case of fat suppression failure, no quantitative measurements are possible for voxels containing both fat and water. Nevertheless, the measurements of  $T_1$  on breast lesions are likely to be less affected by fat suppression failure than the measurements on breast parenchyma, as breast tumors are not expected to have a significant fat content.

Comparing lobular carcinomas and invasive ductal carcinomas, we found later enhancement for lobular carcinomas in

our cohort, in accordance with previous studies,<sup>8,9</sup> but these differences were not statistically significant. Also, similar peak-enhancement was found for the two cancer groups, in agreement with Mann *et al.*<sup>8</sup>  $T_1$  relaxation time is tissue specific and having a quantitative method to measure it allowed the analysis to go further and interpret the distribution of the  $T_1$  values for the lobular and ductal carcinomas. Significant differences in the IQR for  $T_{1\text{peak}}$  and  $T_{1\text{post}}$  between the two patient groups were detected, potentially reflecting their distinct growth and invasion patterns. Lobular cancers may grow in a loosely cohesive manner invading surrounding tissue, whereas ductal cancers usually follow a self-contained solid growth pattern.<sup>17</sup> Ductal carcinomas are therefore more likely to present similar characteristics within a patient population. Figure 4 aims to demonstrate that contrast agent uptake is not necessarily proportional to ER, which is only semiquantitative. In only one of the cases presented, contrast agent uptake rises approximately monotonically with increasing ER, and this could be attributed to differences in the baseline  $T_1$  values between the two tumors. However, the effects of noise and their dependence on  $T_1$  cannot be excluded. The supplementary figure also demonstrates the relationship between ER and [Gd] post-enhancement for lesions with different native  $T_1$  values.

We acknowledge the limitations of this study on a small number of subjects; however, our scope was to demonstrate the potential of the proposed approach. We detected significant differences in the range of  $T_1$  values post-contrast between lobular and ductal carcinomas, but no significant differences between the range of contrast agent concentration values or enhancement ratio values. These findings merit further investigation, as  $T_1$  values could be proposed as independent biomarkers and be directly related to other tumor characteristics in larger cohorts.

Although the sequences employed complied with the DCE-MRI national guidelines for temporal resolution, we cannot exclude that some variations observed might be system and protocol dependent. Qualitative assessment of the enhancement curves may be reader dependent leading to inconsistent interpretation of uptake in tumors.<sup>3</sup> In

quantitative studies, many variations can also arise from different MR systems and DCE sequence parameters.<sup>18–21</sup> Ledger *et al.* highlighted the effect of flip angle and k-space sampling on fat suppression efficiency, dynamic range, and therefore the relationship between signal intensity and  $1/T_1$  for the range of the expected  $T_1$  values.<sup>12</sup> Therefore, the proposed method for quantitative  $T_1$  measurements in fat-suppressed DCE may also need to be validated for other sequence parameters and in other systems. Further work is currently in progress.

In conclusion, fat-suppressed  $T_1$  measurements are viable in breast DCE, resulting in quantitative measurements of contrast agent uptake. The proposed quantitative approach enables the optimization of DCE protocols by tailoring the dynamic range of the sequence to the values of  $T_1$  measured for each population.  $T_1$  measurements from clinical fat-suppressed DCE demonstrated the variations in the  $T_1$  range between ductal and lobular cancer within a relatively small number of patients. This work has demonstrated the feasibility of fat-suppressed  $T_1$  measurements as a tool for clinical studies.

## ACKNOWLEDGMENTS

This article presents independent research partially funded by the CR-UK Cancer Imaging Centre (C1060/A10334) and carried out at the National Institute for Health Research (NIHR) Royal Marsden Clinical Research Facility in association with the NIHR Biomedical Research Centre. The views expressed are those of the author(s) and not necessarily those of the NHS, the NIHR, or the Department of Health.

## APPENDIX 1

### $T_1$ MEASUREMENTS ON RADIOLOGICALLY NORMAL FIBROGLANDULAR TISSUE.

The purpose of this section is to provide further evidence to support the clinical use of our proposed method

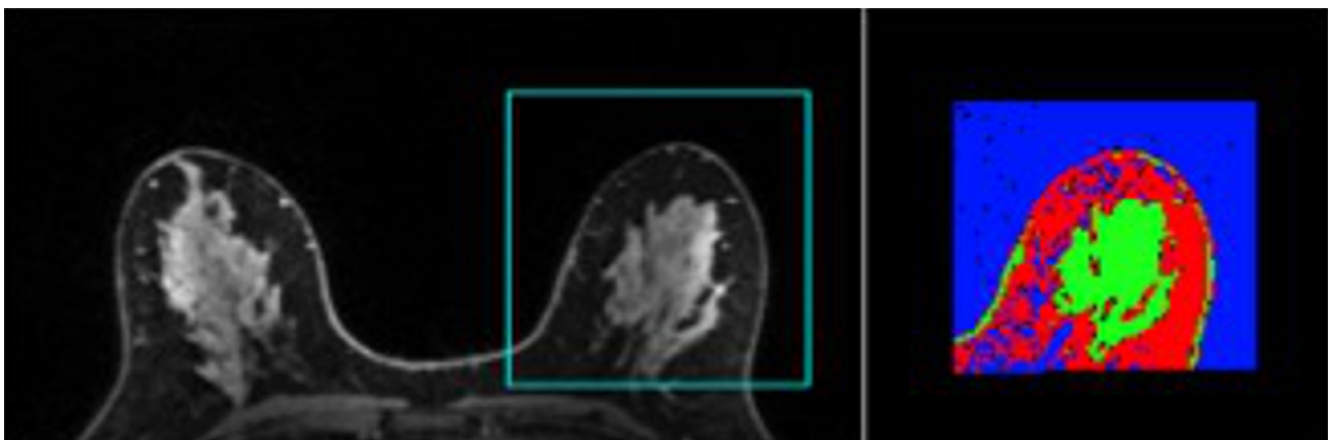


FIG A1. Segmentation of the contralateral breast of a patient with invasive lobular carcinoma on the right breast. Within ROI, three clusters were assigned to fat (red), fibroglandular tissue (green) and background (blue). [Color figure can be viewed at [wileyonlinelibrary.com](http://wileyonlinelibrary.com)]



TABLE A1. Median  $T_1$  values of the contralateral normal-appearing breast tissue.

Subject	Median $T_1$ (ms)
1	1036
2	1130
3	1319
4	1069
5	751
6	635
7	757
8	507
9	1501
10	629
11	881
12	952
13	689
14	1410

for  $T_1$  measurements. The radiologist's reports on the contralateral side of the 20 tumours considered in this study were scrutinized, and the radiologically normal breasts ( $n = 14$ ) were selected. The method proposed in this article to calculate  $T_1$  relaxation time was applied to the normal-appearing contralateral breast fibroglandular tissue. The remaining 6 patients had multifocal disease, benign lesions or random findings on their contralateral breast and therefore were excluded from the analysis. The fibroglandular tissue was segmented on a central PD image by applying clustering segmentation (IDL 8.4 Boulder, CO, USA) to a manually selected ROI containing the contralateral breast (Fig. A1).

The segmented DCE and PD datasets were combined and the  $T_1$  was calculated on a pixel-by-pixel basis before contrast administration, using the test-object calibration curves as described in the Methods section. Table A1 reports the median  $T_1$  of the contralateral fibroglandular tissue for each patient. The average  $T_1$  is  $947 \pm 310$  ms (mean  $\pm$  standard deviation).

The calculated values using the proposed approach are close to previously reported values at 1.5T by Rakow-Penner et al. They employed inversion-recovery to measure the  $T_1$  of normal fibroglandular tissue on regions with high tissue homogeneity.<sup>22</sup> The subjects of our study, however, cover a wide range of ages, hormonal status and were not scanned in the same hormonal phase. Although our measurements include the entire fibroglandular tissue on a central slice, thus considering tissue density variations within the breast, the broad agreement with the literature<sup>22-25</sup> supports the clinical use of our method.

\*These authors contributed equally to this work.

<sup>a)</sup>Author to whom correspondence should be addressed. Electronic mail: eva.kousi@icr.ac.uk.

## REFERENCES

- Turnbull LW. Dynamic contrast-enhanced MRI in the diagnosis and management of breast cancer. *NMR Biomed*. 2009;22:28–39.
- Schnall MD, Blume J, Bluemke DA, et al. Diagnostic architectural and dynamic features at breast MR imaging: multicenter study. *Radiology*. 2006;238:42–53.
- El Khouli RH, Macura KJ, Jacobs MA, et al. Dynamic contrast-enhanced MRI of the breast: quantitative method for kinetic curve type assessment. *Am J Roentgenol*. 2009;193:W295–W300.
- Radjenovic A, Dall BJ, Ridgway JP, Smith MA. Measurement of pharmacokinetic parameters in histologically graded invasive breast tumours using dynamic contrast-enhanced MRI. *Br J Radiol*. 2008;81:120–128.
- Ah-See ML, Makris A, Taylor NJ, et al. Early changes in functional dynamic magnetic resonance imaging predict for pathologic response to neoadjuvant chemotherapy in primary breast cancer. *Clin Cancer Res*. 2008;14:6580–6589.
- Veltman J, Boetes C, Van Die L, Bult P, Blickman JG, Barentsz JO. Mammographic detection and staging of invasive lobular carcinoma. *Clin Imaging*. 2006;30:94–98.
- Watermann DO, Tempfer C, Hefler LA, Parat C, Stickeler E. Ultrasound morphology of invasive lobular breast cancer is different compared with other types of breast cancer. *Ultrasound Med Biol*. 2005;31:167–174.
- Mann RM, Veltman J, Huisman H, Boetes C. Comparison of enhancement characteristics between invasive lobular carcinoma and invasive ductal carcinoma. *J Magn Reson Imaging*. 2011;34:293–300.
- Dietzel M, Baltzer PA, Vag T, et al. Magnetic resonance mammography of invasive lobular versus ductal carcinoma: systematic comparison of 811 patients reveals high diagnostic accuracy irrespective of typing. *J Comput Assist Tomogr*. 2010;34:587–595.
- Clayton D, Davison C, Bailey C, et al. Technical guidelines for magnetic resonance (MRI) for the surveillance of women at higher risk of developing breast cancer. (NHSBSP Publication No 68, 2012).
- Wang HZ, Riederer SJ, Lee JN. Optimizing the precision in  $T_1$  relaxation estimation using limited flip angles. *Magn Reson Med*. 1987;5:399–416.
- Ledger AEW, Borri M, Pope RJ, et al. Investigating the influence of flip angle and k-space sampling on dynamic contrast-enhanced MRI breast examinations. *Acad Radiol*. 2014;21:1394–1401.
- Azlan CA, Di Giovanni P, Ahearn TS, Semple SIK, Gilbert FJ, Redpath TW. B1 transmission-field inhomogeneity and enhancement ratio errors in dynamic contrast-enhanced MRI (DCE-MRI) of the breast at 3T. *J Magn Reson Imaging*. 2010;31:234–239.
- Kousi E, Borri M, Dean J, et al. Quality assurance in MRI breast screening: comparing signal-to-noise ration in dynamic contrast-enhanced imaging protocols. *Phys Med Biol*. 2011;1:37–49.
- Schmidt MA, Borri M, Scurr E, et al. Breast dynamic contrast-enhanced examinations with fat suppression: are contrast-agent uptake curves affected by magnetic field inhomogeneity? *Eur Radiol*. 2013;23:1537–1545.
- Hancu I, Govenkar A, Lenkinski RE, Lee SK. On shimming approaches in 3T breast MRI. *Magn Reson Med*. 2013;69:862–867.
- Schnitt SJ, Guidi AJ. Pathology of invasive breast cancer. In: *Diseases of the Breast* (3rd ed). Philadelphia, PA: Lippincott Williams & Wilkins; 2004.
- Jansen SA, Shimauchi A, Zak L, et al. Kinetic curves of malignant lesions are not consistent across MRI systems: need for improved standardization of breast dynamic contrast-enhanced MRI acquisition. *Am J Roentgenol*. 2009;193:832–839.
- Pabst T, Kenn W, Kaiser WA, Hahn D. Understanding why contrast enhancement in dynamic MRI is not reproducible: illustration with a simple phantom. *Breast J*. 2001;7:166–170.
- Kuhl C. The current status of breast MR imaging - Part I. Choice of technique, image interpretation, diagnostic accuracy, and transfer to clinical practice. *Radiology*. 2007;244:356–378.
- Moon M, Cornfeld D, Weinreb J. Dynamic contrast-enhanced breast MR imaging. *Magn Reson Imaging Clin N Am*. 2009;17:351–362.
- Rakow-Penner R, Daniel B, Yu H, Sawyer-Glover A, Glover G. Relaxation times of breast tissue at 1.5T and 3T measured using IDEAL. *J Magn Reson Imaging*. 2006;23:87–91.
- Delille JP, Slanetz PJ, Yeh ED, Kopans ED, Gerrido L. Physiologic changes in breast magnetic resonance imaging during the menstrual

cycle: perfusion Imaging, signal enhancement, and influence of the T1 relaxation time of breast tissue. *Breast J.* 2005;11:236–241.

24. Edward RE. *Breast MRI: Fundamentals and Technical Aspects*. New York, NY: Springer Science + Business Media; 2008.
25. Merchant TE, Thelissen GRP, de Graaf PW, Nieuwenhuizen CWA, Kievit HCE, Den Otter W. Application of a mixed imaging sequence for MR imaging characterisation of human breast disease. *Acta Radiol.* 1993;34:356–361.

## SUPPORTING INFORMATION

Additional Supporting Information may be found online in the supporting information tab for this article.

**Fig. S1.** %Enhancement Ratio versus [Gd] and native T1 distribution for different lesions.